Noisy Single Image Super-Resolution Based on Local Fractal Feature Analysis

KAI SHAO[1], **QINGLAN FAN**[2], **YUNFENG ZHANG**[1], **FANGXUN BAO**[3],
AND CAIMING ZHANG[4]

[1]School of Computer Science and Technology, Shandong University of Finance and Economics, Jinan 250014, China
[2]School of Engineering and Computer Science, Victoria University of Wellington, Wellington 6012, New Zealand
[3]School of Mathematics, Shandong University, Jinan 250100, China
[4]School of Computer Science and Technology, Shandong University, Jinan 250100, China

Corresponding author: Qinglan Fan (fan_qinglan@163.com)

ABSTRACT Generally, most existing super-resolution (SR) methods do not consider noise, which treats SR reconstruction and denoising as two separate problems and performs separately. However, noise is inevitably introduced in the imaging process. Based on analysis of the degraded model, in this paper, the problems of interpolation and denoising are modeled to estimate the noiseless and missing images under the same framework. By applying local fractal dimension (LFD) into image local feature analysis, a noisy single-image SR method is proposed. For each noisy image, we first construct a rational fractal interpolation model containing scaling factors, which can effectively maintain the inherent properties of the data. Furthermore, the original image structure can be well preserved by applying the interpolation model. Considering the local characteristics of the image, scaling factors are calculated on the basis of the LFDs. Then, through further local feature analysis of the interpolated image, a denoising method based on LFD is proposed for recovering a noiseless image. Finally, a high-quality high-resolution image is obtained. Experimental results demonstrate that our method outperforms the state-of-the-art methods both quantitatively and qualitatively.

INDEX TERMS Noisy image super-resolution, local fractal dimension, local fractal feature analysis, scaling factors.

I. INTRODUCTION

Image restoration (IR) aims to reconstruct a high-quality image from its degraded version. IR is an ill-posed inverse problem [1] for an observed image, and it can be modeled as

$$y = DHx + v, \tag{1}$$

where x is the original image, D is down-sampling operator, H is blur kernel, and v is additive noise. When H is not considered, the IR problem reduces to a super-resolution (SR) problem. Typically, the existing SR methods can be broadly classified into three categories: interpolation-based methods, reconstruction-based methods, and learning-based methods.

Interpolation-based methods are considered a relatively basic approach to SR and usually utilize a basic function of interpolation kernel to estimate the unknown pixels in the

high-resolution (HR) image. Traditional interpolation algorithms, including nearest point interpolation, bilinear interpolation and bicubic interpolation [2], are simple. However, these methods tend to generate zigzag artifacts along edges. To improve the performance of traditional methods, many other adaptive interpolation methods [3], [4] have been proposed. Although these types of methods can preserve sharper edges, they often produce speckle noise or distortion in texture regions.

Reconstruction-based methods [5]–[7] generally rely on a certain amount of prior knowledge during the reconstruction process. Such methods can maintain the image edge structure and avoid aliasing artifacts, but the quality of the reconstructed image can promptly degrade (such as over smoothing, the loss of significant high-frequency details) when the required magnification factor is large.

Learning-based methods [8]–[10] recover missing high-frequency details by exploiting the mapping relationship
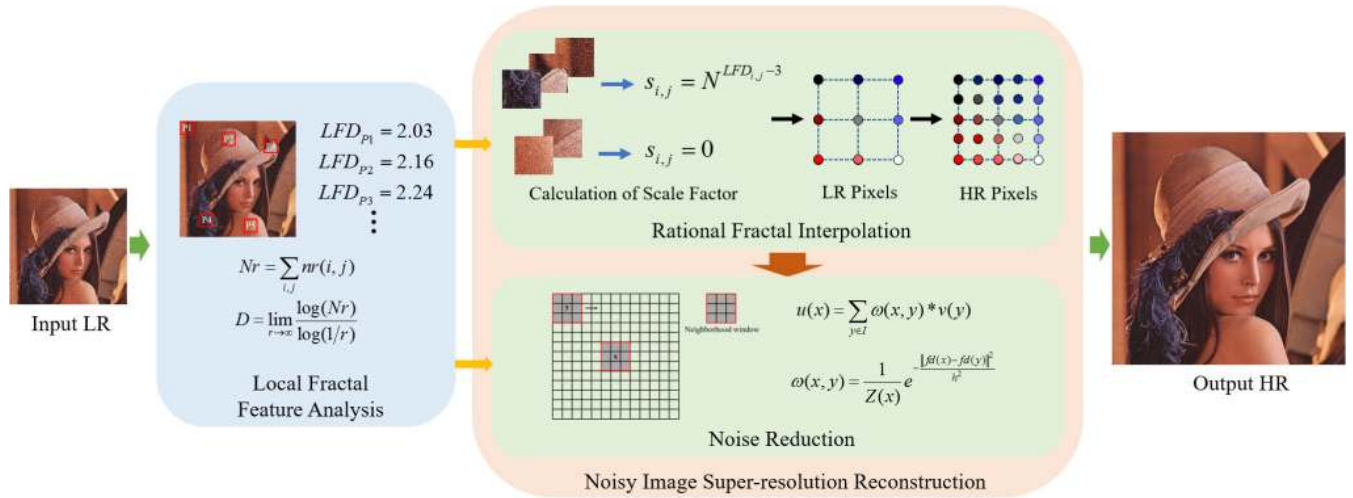
The associate editor coordinating the review of this manuscript and approving it for publication was Nilanjan Dey [ID].

FIGURE 1. Algorithm framework.

between low-resolution (LR) and HR image pairs. These algorithms are generally applicable to a certain category of images, but they are fixed and therefore not suitable for the input image. Moreover, if the LR images do not contain sufficient repeating patterns, these algorithms use similarity redundancy information to generate the HR images, which is prone to generate sharpened edges instead of fine details.

Most of the existing SR methods assume that the image to be reconstructed is noiseless. However, this assumption is invalid in practical applications because noise will inevitably be introduced in the process of image acquisition, which makes the SR problem more challenging. Sparse representation schemes are used for reconstructing images in [11], [12]. The abovementioned methods are still more robust to input noise by transforming the problem into sparse representation model, but they are effective only on the condition that the input LR images are corrupted by a small amount of noise. Another common strategy for dealing with noisy data [13], [14] is to divide the restoration process into two disjoint steps: denoising and interpolation. Instead of performing denoising and interpolation separately, a third strategy [15] is to treat both tasks as estimation problem, which can yield better subjective visual quality.

According to the above descriptions and discussion, preserving the texture details and structural information is a critical task in image SR processing that is based on degraded model analysis. In recent years, fractal analysis has served as the basis of a valid texture descriptor in texture classification and segmentation [16], [17]. Consequently, fractal analysis has attracted increasing attention in the SR literature because of its ability to precisely characterize textures. Wee *et al.* [18] proposed a fast fractal SR technique using fractal coding, which can preserve image details well but fails to restore sharp edges. Xu *et al.* [19] presented a single-image SR and enhancement algorithm utilizing local fractal analysis. This method can effectively enhance the image details, but it cannot obtain satisfactory results in random texture region

that do not conform to the local fractal characteristics. It should be noted that the fractal analysis methods mentioned above mainly use the fractal dimension [20] to characterize the texture features.

In this paper, a new single-image SR algorithm is proposed to estimate both the noise-free and missing images from noisy images using local fractal feature analysis. The main steps of the proposed algorithm are shown in Fig. 1. For a given noisy image, first, the local features of the image are analyzed in terms of the local fractal dimension (LFD) [21]. Then, scaling factors are calculated using the LFD features, and the LR image is adaptively magnified by using a corresponding interpolation model. Finally, an image denoising method based on local fractal features is proposed to obtain a high-quality HR image.

The main contributions of the proposed method are summed up as follows:

(1) Under the framework of local fractal feature analysis, we develop a noisy image SR method, that performs interpolation and denoising in tandem. The proposed approach can accurately restore the spatial feature information of images, achieving good preservation of texture regions in particular.

(2) A new rational fractal interpolation model is constructed. First, compared with the existing interpolation methods, the proposed interpolation model can more effectively describe image features. In addition, it has a certain degree of noise immunity.

(3) The fractal dimension reflects the complexity of image texture information. Based on the relationship between the scaling factor and the LFD, a method of accurately calculating scaling factors is proposed. Based on the LFD, an effective image denoising method is presented.

II. RELATED WORKS
Numerous noisy image SR methods have been studied in the computer vision community. Some noisy image SR methods are based on single-image SR methods. To improve the

performance of interpolation-based SR methods, a fast image upsampling method was proposed [4]. Although this method retains sharp edges, noise is introduced in the reconstruction process. Huang *et al.* [10] proposed a single image SR method via multiple mixture prior models, which not considered noise in the process of image SR. However, noise will inevitably be introduced during image processing, so it is necessary to consider the influence of noise in image SR processing. Regarding sparse representation schemes, Dong *et al.* [11] proposed a sparse representation-based image SR method by using adaptive sparse domain selection and adaptive regularization. Mandal *et al.* [12] developed a noise-adaptive single image SR method in sparse representation framework. These two sparse representation methods can obtain satisfactory results only when the noise intensity is low.

Other methods divide the noisy image SR process into two disjoint steps, including denoising and interpolation. Although these methods can handle noise fairly well, the reconstructed results are not satisfactory in terms of preserving image features since the denoising process may introduce some artifacts, which can be further amplified in the interpolation phase. Zhang *et al.* [15] proposed a directional denoising and interpolation algorithm that treats denoising and interpolation as estimation problems. The image edge structure can be well preserved with this method, but the recovered texture details are not ideal. Zhang *et al.* [22] proposed an IR method by plugging the deep denoiser prior as a modular part into a half quadratic splitting based iterative algorithm. For the task of noisy image SR with a high noise intensity, this method cannot effectively remove noise while maintaining sufficient texture detail information. To maintain texture details, Zhang *et al.* [23] proposed a single-image SR algorithm which applied the fractal analysis method to image interpolation by constructing rational fractal interpolation function (FIF). This type of method shows advantages in comparison to other SR reconstruction techniques, especially in terms of preserving fine image details and textural features. In this paper, we construct a new type of rational fractal interpolation model to achieve noisy image SR. Compared with the interpolation model presented in [23], our proposed model has better nonlinear properties and can maintain the inherent properties and original structure of the image data making it more suitable for noisy image reconstruction.

III. IMAGE LOCAL FRACTAL FEATURE ANALYSIS

In general, natural images contain smooth, edge and texture regions, indicating that the measurement of the natural image is locally adaptable. Thus, a local feature analysis method may be more appropriate than global analysis for natural image processing. Most natural images can be represented as a fractal set, and fractal theory has been widely applied in image processing technology [24]. In feature analysis based on fractal theory, the fractal dimension is used to describe the features of an image. LFD can more accurately describe the local geometric structure of an image. In this paper, by introducing the LFD into local feature analysis, we achieve SR results in which texture regions do not contain artifacts such as fuzziness and distortion. Fractal analysis can be used to correctly describe the spatial features of an image. The fractal dimension is essentially determined by the fractal measure, which is an important parameter for characterizing image roughness. The box-counting dimension of fractals is one of the most commonly used fractal dimensions, which is convenient for mathematical calculation and empirical estimation. Thus, we will introduce how to compute the LFD and the fractal dimension for the images.

Consider the image as a curved surface in 3-D space, where two coordinates (x, y) represent 2-D plane position and the third coordinate (z) represents the pixel value. For a given image of size $M \times M$, we partition the 3-D space into boxes of sides $s \times s \times s$, where $r = M/s$ represents the number of boxes needed to cover a row or column of the image. Suppose that the minimum and maximum values of image pixels in the grid (i, j) are in the box u and box v respectively, then $nr(i, j) = v - u + 1$ is the number of boxes required to cover the image in the grid (i, j). Further, the number of boxes required to cover the entire image is Nr,

$$Nr = \sum_{i,j} nr(i, j), \qquad (2)$$

then the fractal dimension of the whole image is

$$D = \lim_{r \to \infty} \frac{log(Nr)}{log(1/r)}. \qquad (3)$$

The LFD of entire image can be obtained by computing the fractal dimension from local region for each image patch.

IV. NOISY IMAGE SUPER-RESOLUTION RECONSTRUCTION ALGORITHM

The proposed reconstruction algorithm is based on analysis of the degraded model, namely, upsampling and denoising. In this paper, both interpolation and denoising are treated as estimation problems, and noise-free and missing image information is estimated within the framework of local fractal feature analysis.

A. IMAGE INTERPOLATION

Interpolation is a basic problem of resampling image size in image processing [25]. Compared with linear methods, nonlinear methods are more suitable for image interpolation [14]. Furthermore, the fractal is an efficient model of texture. Here, we construct a rational fractal interpolation model.

1) CONSTRUCTION OF INTERPOLATION MODEL

Let $\Omega = [a, b; c, d]$ be the plane region, and $\{(x_i, y_j, f_{i,j}, d_{i,j}^*, d_{i,j}) : i = 1, 2, \cdots, N; j = 1, 2, \cdots, M\}$ be a given set of data points, where $a = x_1 < x_2 < \ldots < x_N = b, c = y_1 < y_2 < \cdots < y_M = d$ are the knot spacings, $f_{i,j}$ represents the value of $f(x, y)$ at the point (x_i, y_j). Let $d_{i,j}^*$ and $d_{i,j}$ be chosen partial derivative values $\frac{\partial f(x,y)}{\partial x}$ and $\frac{\partial f(x,y)}{\partial y}$ at the knots (x_i, y_j), respectively. Denote $h_i = x_{i+1} - x_i$,

$l_j = y_{j+1} - y_j$, and for any point $(x, y) \in [a, b; c, d]$, $\theta := \frac{x - x_1}{x_N - x_1}$, $\eta := \frac{y - y_1}{y_M - y_1}$.

Denote

$$\omega_{0,0}(\theta) = \frac{(1 - \theta)^2(1 + \theta)}{1 - \theta + \theta^3}, \quad \omega_{0,1}(\theta) = \frac{\theta^2}{1 - \theta + \theta^3},$$

$$\omega_{1,0}(\theta) = \frac{\theta(1 - \theta)^2}{1 - \theta + \theta^3}, \quad \omega_{1,1}(\theta) = \frac{-\theta^2(1 - \theta)}{1 - \theta + \theta^3}. \quad (4)$$

Now, we consider the following iterated function system (IFS),

$$\begin{cases} \varphi_i(x) = a_i x + b_i, \\ \psi_j(y) = c_j y + d_j, \\ F_{i,j}(x, y, z) = s_{i,j} z + P_{i,j}(\varphi_i(x), \psi_j(y)) \\ \quad - s_{i,j} B_{i,j}(x, y). \end{cases} \quad (5)$$

where $|s_{i,j}| < 1$, $a_i = \frac{x_{i+1} - x_i}{x_N - x_1}$, $b_i = \frac{x_N x_i - x_i x_{i+1}}{x_N - x_1}$, $c_j = \frac{y_j - y_1}{y_M - y_1}$, $d_j = \frac{y_M y_j - y_1 y_{j+1}}{y_M - y_1}$, and

$$\begin{aligned} P_{i,j}(\varphi_i(x), \psi_j(y)) &= a_{r,s}(\theta, \eta) f_{i+r, j+s} \\ &+ b_{r,s}(\theta, \eta) h_i d^*_{i+r, j+s} \\ &+ c_{r,s}(\theta, \eta) l_j d_{i+r, j+s}, \quad (6) \\ B_{i,j}(x, y) &= a_{r,s}(\theta, \eta) f_{r(N-1)+1, s(M-1)+1} \\ &+ b_{r,s}(\theta, \eta) H_N d^*_{r(N-1)+1, s(M-1)+1} \\ &+ c_{r,s}(\theta, \eta) L_M d_{r(N-1)+1, s(M-1)+1}, \quad (7) \end{aligned}$$

with

$$\begin{aligned} a_{r,s}(\theta, \eta) &= \omega_{0,r}(\theta) \omega_{0,s}(\eta), \\ b_{r,s}(\theta, \eta) &= \omega_{1,r}(\theta) \omega_{0,s}(\eta), \\ c_{r,s}(\theta, \eta) &= \omega_{0,r}(\theta) \omega_{1,s}(\eta), \quad (8) \end{aligned}$$

then the IFS $\{I \times J \times R; (\varphi_i(x), \psi_j(y), F_{i,j}(x, y, z))\}$ defined by (5) allows a particular attractor G, and G is the graph of a continuous function $\Phi(x, y)$, which satisfies

$$\begin{aligned} \Phi(\varphi_i(x), \psi_j(y)) &= F(x, y, \Phi(x, y)) = s_{i,j} \Phi(x, y) \\ &+ P_{i,j}(\varphi_i(x), \psi_j(y)) - s_{i,j} B_{i,j}(x, y), \\ i &= 1, 2, \cdots N-1; \ j = 1, 2, \cdots, M-1. \end{aligned} \quad (9)$$

$s_{i,j}$ is called scaling factor of the IFS. Further, the rational FIF $\Phi(x, y)$ defined by (9) is C^1-continuous if $|s_{i,j}| < \min\{a_i, c_j\}$. The terms $\{(a_{r,s}(\theta, \eta), b_{r,s}(\theta, \eta), c_{r,s}(\theta, \eta)) : r = 0, 1; s = 0, 1\}$ are called the symmetric bases of the bivariate rational FIF defined by (9), which satisfy

$$\sum_{s=0}^{1} \sum_{r=0}^{1} a_{r,s}(\theta, \eta) = 1. \quad (10)$$

2) SCALING FACTOR CALCULATION BASED ON LFD

The interpolation surface has different shapes with diverse values of the scaling factors. When the value of the scaling factor is higher, the corresponding interpolation surface is more complex. Meanwhile, different LFD corresponds to different areas of the image. An image region with a more
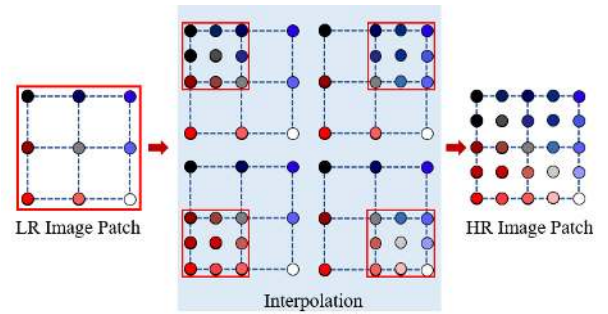

FIGURE 2. The interpolation process of rational fractal interpolation model.

complex texture has a larger LFD, whereas the pixel values in a smooth region change relatively little. The relationship between the fractal dimension and the scaling factors of the constructed fractal surface is shown in (11),

$$\sum_{i=1}^{N} \sum_{j=1}^{N} |s_{i,j}| a_i^{D-2} c_j = 1, \quad (11)$$

where D is the box-counting dimension of fractal surface defined by (9). For images, $a_i = c_j = \frac{1}{N}$.

According to formula (11), the fractal dimension of the surfaces is closely related to the values of scaling factors in the corresponding bivariate rational FIF. The purpose of this paper is to use surface interpolation to recover a high-quality HR image from one LR image. Considering the local geometric structure of an image, according to formula (11), the scaling factors of each image patch are given, namely,

$$s_{i,j} = N^{LFD_{i,j} - 3}. \quad (12)$$

3) INTERPOLATION ALGORITHM

With different scaling factors, the constructed rational FIF can take different forms for describing and processing an image. Based on the local fractal feature analysis of the original image, the proposed model is applied for image interpolation.

Our interpolation algorithm consists of three parts: (1) Decompose LR image into patches of size 3×3. (2) Interpolate each image patch individually. (3) Integrate these image patches into the HR image. For every LR image patch, as is shown in Fig. 2, the missing HR samples can be obtained by constructed interpolation function. The basic idea of this method is to structure the interpolation surface using a 3×3 vector control mesh, and then obtain the intensity of every point in the HR image. More specifically, a fractal is a shape composed of parts that is somewhat similar to the whole, as is shown in Fig. 2, the pixels in the red rectangle (3×3) are computed by using 3×3 LR image pixels. For the entire image, there is an overlapping pixel point between the patches in the processing to ensure a smooth connection among patches. Further, the interpolation is completed by traversing each patch in raster-scan order in the LR image.

By applying constructed interpolation model into noise image interpolation, the initial HR image patches can be obtained, in which the structural characteristics of original texture can be reserved as well as more image details can be recovered. To obtain a clearer HR image, it is necessary to filter image noise. Preserving image texture and structure information is a critical issue in image denoising.

B. IMAGE DENOISING

The majority of existing denoising methods are based on averaging the pixels in the image to achieve a denoising effect; however, these approaches tend to cause the loss of image details during the denoising process. The non-local means algorithm (NL-means) [26] utilizes the redundant information in the image to filter out noise, and it preserves image details well. However, when the method incorrectly selects similar points, the details of image information will not be preserved well, which is especially common in images with complex textures. Instead, a fractal can describe the spatial characteristic information of the image correctly. The LFD is an important parameter that characterizes the amount of roughness in an image. Thus, we propose a NL-means denoising algorithm based on LFD that combines LFD with the local mean to search for and correctly select similar points. The process of the denoising algorithm is shown in Algorithm 1. This approach performs a better denoising effect and preserves the texture and structure information of the image.

In Figure 3, the large window is a search window centered on the target pixel x, and the two grey small windows are neighborhood windows centered on x and y, respectively. The neighborhood window centered on y moves within the search window, and each pixel x is computed as the weighted average of the pixels that have structures similar to x in the search window. Namely, given a noisy image v, the denoised image is:

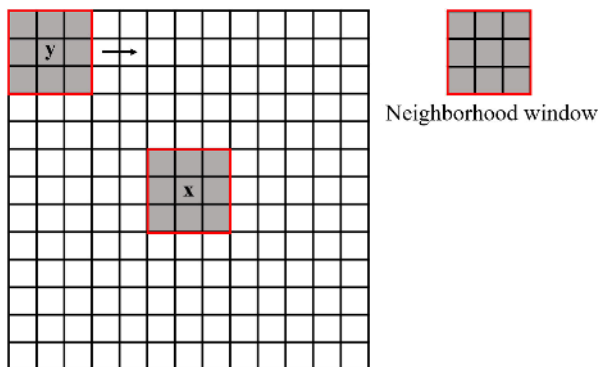$$u(x) = \sum_{y \in I} \omega(x, y) * v(y), \qquad (13)$$

Algorithm 1 NL-Mean Denoising Algorithm Based on LFD

Input: Original image set $v(i, j, z(i, j), d)$, the size of an image is $M \times M$, i, j represent the row and column coordinate of the pixel x and y, $z(i, j)$ is grey value, d is the number of image;

Output: Denoised image set $u(i, j, z(i, j), d)$;

1: initialize the size of search window is $S \times S$, search step is 1;
2: **for** $t = 1 : d$ **do**
3:     **for** $i = 1 : M$ **do**
4:         **for** $j = 1 : M$ **do**
5:             **for** $ii = 1 : S$ **do**
6:                 **for** $jj = 1 : S$ **do**
7:                     **if** $\left| LFD_{x(i,j)} - LFD_{y(ii,jj)} \right| \leqslant T$ **then**
8:                         compute $\omega(x, y)$ by (14);
9:                     **end if**
10:                 **end for**
11:             **end for**
12:             compute $z(i, j)$ by (13);
13:         **end for**
14:     **end for**
15:     obtain the denoised image $u(i, j, z(i, j))$;
16: **end for**
17: obtain the denoised image set $u(i, j, z(i, j), d)$;

---

where the family of weights $\{\omega(x, y)\}_y$ depend on the similarity between x and y and satisfy the usual conditions, i.e., $0 \leqslant \omega(x, y) \leqslant 1$ and $\sum_y \omega(x, y) = 1$. I represents the pixels in the search window.

To effectively preserve image edges and complex textures during denoising, the first task is to search for the correct similar points for pixel x with the help of the LFD. The LFD can reflect the roughness of the image block. Therefore, the threshold T is used to filter out dissimilar image blocks based on LFD. Let LFD_x be the fractal dimension of pixel x. When $\left| LFD_x - LFD_y \right| > T$, $\omega(x, y) = 0$; when $\left| LFD_x - LFD_y \right| \leqslant T$, the similarity as a decreasing function of the weighted euclidean distance:

$$\omega(x, y) = \frac{1}{Z(x)} e^{-\frac{\left\| LFD_x - LFD_y \right\|^2}{h^2}}, \qquad (14)$$

where $Z(x)$ is a normalizing constant calculated as follows:

$$Z(x) = \sum_y e^{-\frac{\left\| LFD_x - LFD_y \right\|^2}{h^2}}, \qquad (15)$$

The parameter h acts as the filtering degree.

V. EXPERIMENTAL RESULTS

To illustrate the effectiveness of the presented algorithm, we conducted experiments on the Set5 [27], Set14 [28] and Kodak [1] datasets and selected eight SR algorithms to compare experiment results with the scaling factor of $\times 2$. These methods are bicubic interpolation, MMPM [10], Zhang's [23],

---

[1] http://r0k.us/graphics/kodak/

FIGURE 3. The sliding process of the neighborhood window in the search window.

TABLE 1. Objective quality assessment of different methods on Set5.

Image	Noise	Index	Bicubic	MMPM [10]	Zhang's [23]	US [4]	LMMSE [15]	ASDS [11]	NASR [12]	DPIR [22]	Zhang's + Denoising	Ours
baby	$\sigma=5$	PSNR	30.01	31.94	32.39	31.90	30.01	32.37	30.51	30.24	33.08	**33.22**
		SSIM	0.828	0.921	0.94	0.923	0.939	0.902	0.882	0.935	**0.944**	0.942
bird	$\sigma=5$	PSNR	30.97	31.04	31.09	30.77	30.97	31.95	30.78	29.53	31.93	**32.04**
		SSIM	0.710	0.902	0.904	0.884	0.900	0.874	0.859	0.897	0.908	**0.912**
butterfly	$\sigma=5$	PSNR	25.56	25.51	25.47	24.91	25.56	**26.78**	24.49	24.38	25.52	25.56
		SSIM	0.660	0.874	0.869	0.862	0.879	0.880	0.845	0.858	0.875	**0.883**
head	$\sigma=5$	PSNR	27.75	28.76	29.63	29.42	27.75	29.42	27.97	28.90	29.87	**29.91**
		SSIM	0.592	0.758	0.761	0.718	0.745	0.687	0.648	0.769	0.770	**0.772**
women	$\sigma=5$	PSNR	29.12	29.42	29.38	28.40	29.12	**30.64**	28.56	29.21	30.56	30.52
		SSIM	0.689	0.895	0.889	0.865	0.888	0.876	0.849	0.896	0.902	**0.910**
average	$\sigma=5$	PSNR	28.68	29.33	29.59	29.08	28.68	30.23	28.46	28.45	30.19	**30.25**
		SSIM	0.695	0.870	0.872	0.850	0.870	0.843	0.816	0.871	0.880	**0.884**
baby	$\sigma=10$	PSNR	28.32	30.26	29.88	29.39	28.32	29.38	27.78	29.46	**31.34**	31.32
		SSIM	0.771	0.865	0.885	0.828	0.873	0.782	0.759	0.892	0.898	**0.900**
bird	$\sigma=10$	PSNR	28.88	30.12	29.35	28.61	28.88	29.18	28.38	29.16	30.31	**30.44**
		SSIM	0.627	0.849	0.824	0.774	0.790	0.760	0.740	0.845	0.858	**0.861**
butterfly	$\sigma=10$	PSNR	24.68	24029	23.69	24.12	24.68	**25.51**	23.73	24.40	25.37	25.22
		SSIM	0.601	0.801	0.817	0.785	0.798	0.790	0.753	0.834	0.846	**0.851**
head	$\sigma=10$	PSNR	26.72	27.97	28.11	27.88	26.72	27.70	26.89	28.80	28.90	**29.04**
		SSIM	0.527	0.662	0.676	0.629	0.660	0.596	0.572	0.648	0.671	**0.679**
women	$\sigma=10$	PSNR	27.57	28.18	27.94	27.04	27.57	28.25	26.74	27.09	29.01	**29.03**
		SSIM	0.608	0.864	0.839	0.755	0.780	0.750	0.719	0.857	0.862	**0.866**
average	$\sigma=10$	PSNR	27.23	28.16	27.79	27.40	27.23	28.00	26.70	27.78	28.98	**29.01**
		SSIM	0.626	0.808	0.808	0.754	0.780	0.735	0.708	0.815	0.827	**0.831**
baby	$\sigma=20$	PSNR	25.59	26.90	28.73	24.39	26.28	21.03	25.40	23.08	28.94	**29.01**
		SSIM	0.688	0.630	0.776	0.685	0.763	0.579	0.500	0.749	0.798	**0.805**
bird	$\sigma=20$	PSNR	24.63	26.30	28.52	23.93	25.20	20.83	24.58	23.10	28.57	**28.58**
		SSIM	0.615	0.710	0.720	0.735	0.756	0.654	0.589	0.788	0.802	**0.810**
butterfly	$\sigma=20$	PSNR	19.97	21.22	25.08	22.10	19.57	19.54	20.37	20.02	25.54	**25.79**
		SSIM	0.597	0.752	0.742	0.767	0.764	0.749	0.688	**0.820**	0.793	0.790
head	$\sigma=20$	PSNR	25.86	27.24	28.18	24.92	26.42	21.37	25.91	22.96	28.27	**28.23**
		SSIM	0.516	0.610	0.616	0.619	0.633	0.434	0.479	0.645	0.664	**0.669**
woman	$\sigma=20$	PSNR	22.48	24.40	27.55	22.70	23.21	20.53	22.96	22.03	28.32	**28.46**
		SSIM	0.597	0.684	0.705	0.700	0.776	0.575	0.569	0.753	0.799	**0.811**
average	$\sigma=20$	PSNR	23.70	25.21	27.21	23.60	24.14	20.65	23.84	23.86	27.93	**28.01**
		SSIM	0.602	0.678	0.712	0.701	0.754	0.598	0.565	0.751	0.771	**0.777**

TABLE 2. Objective quality assessment of different methods on Set14.

Noise	Index	Bicubic	MMPM [10]	Zhang's [23]	US [4]	LMMSE [15]	ASDS [11]	NASR [12]	DPIR [22]	Zhang's + Denoising	Ours
$\sigma=5$	PSNR	28.17	29.91	29.98	29.74	28.32	30.01	29.15	29.97	30.04	**30.16**
	SSIM	0.827	0.849	0.852	0.831	0.853	0.844	0.826	0.857	0.861	**0.872**
$\sigma=10$	PSNR	25.16	25.38	25.57	25.44	25.25	25.37	24.58	26.04	26.14	**26.22**
	SSIM	0.693	0.783	0.794	0.778	0.791	0.741	0.714	0.793	0.817	**0.823**
$\sigma=20$	PSNR	22.93	23.87	24.76	22.99	23.14	23.21	23.07	24.29	25.35	**25.56**
	SSIM	0.671	0.744	0.743	0.719	0.727	0.702	0.694	0.761	0.788	**0.798**

US [4], LMMSE [15], ASDS [11], NASR [12] and DPIR [22]. We also carried out experiments by cascading the proposed denoising method after the Zhang's. In all experiments, the original images are added with different levels of Gaussian noise as inputs (The standard deviations of Gaussian noise are 5, 10 and 20 in this paper).
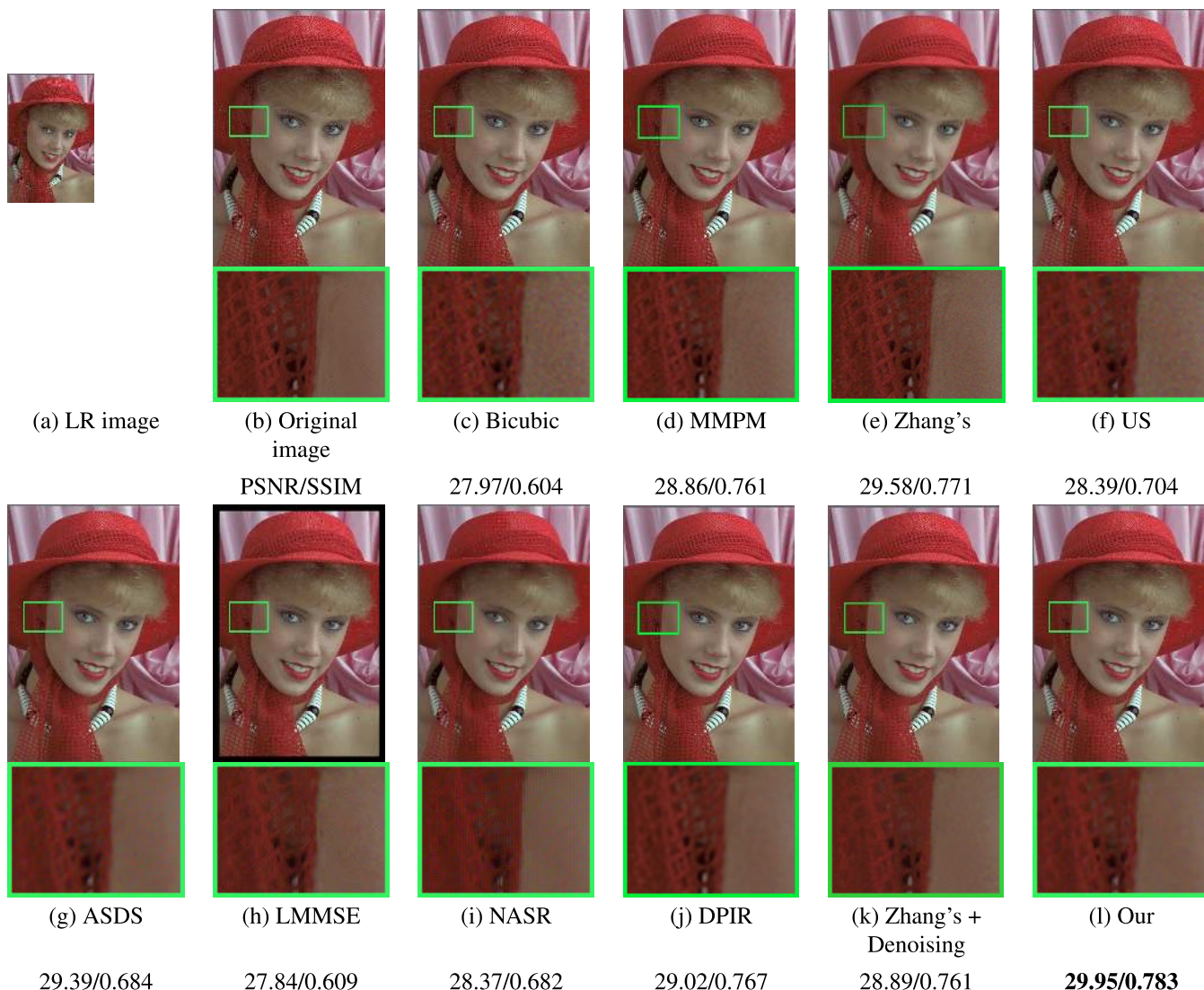
(a) LR image	(b) Original image	(c) Bicubic	(d) MMPM	(e) Zhang's	(f) US
	PSNR/SSIM	27.97/0.604	28.86/0.761	29.58/0.771	28.39/0.704
(g) ASDS	(h) LMMSE	(i) NASR	(j) DPIR	(k) Zhang's + Denoising	(l) Our
29.39/0.684	27.84/0.609	28.37/0.682	29.02/0.767	28.89/0.761	**29.95/0.783**

FIGURE 4. Comparison of SR results on Girl image ($\sigma = 5$).

TABLE 3. Edge preservation index of noiseless images.

Dataset	Bicubic	MMPM [10]	Zhang's [23]	US [4]	LMMSE [15]	ASDS [11]	NASR [12]	DPIR [22]	Zhang's + Denoising	Ours
Set5	0.786	0.805	0.796	0.790	0.787	0.793	0.779	0.808	0.811	**0.821**
Set14	0.662	0.667	0.684	0.679	0.681	0.689	0.663	0.669	0.697	**0.705**

TABLE 4. Comparison of running time for different methods.

Methods	Bicubic	MMPM [10]	Zhang's [23]	US [4]	LMMSE [15]	ASDS [11]	NASR [12]	DPIR [22]	Zhang's + Denoising	Ours
Set5	3.34	0.48	77.69	1.47	6.32	335.74	104.83	84.77	83.67	82.51
Set14	4.04	0.62	84.35	1.83	7.20	423.34	127.17	91.43	92.92	90.75
Average	3.69	0.55	81.02	1.65	6.76	379.54	116.97	88.10	88.30	86.63

A. QUANTITATIVE RESULTS

We employ peak signal-to-noise ratio (PSNR) and structural similarity (SSIM) indices for quantitative comparisons. PSNR is defined as $10 \log 10(255^2/\text{MSE})$, wherein MSE is the mean squared error (MSE) for two monochrome images to be compared. SSIM is an index based on visual perception for evaluating image reconstruction quality. In Tables 1 and 2 we report the average PSNR and SSIM performance of all
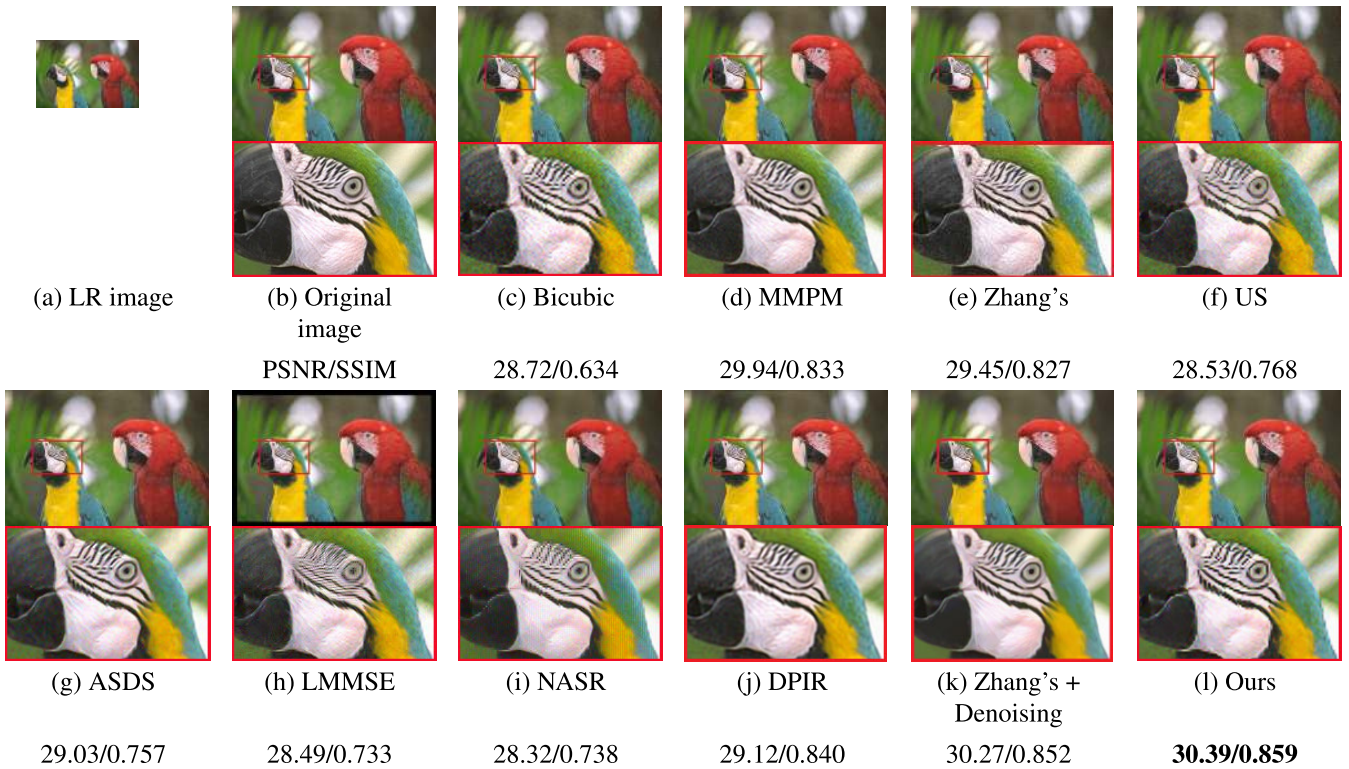
(a) LR image	(b) Original image	(c) Bicubic	(d) MMPM	(e) Zhang's	(f) US
	PSNR/SSIM	28.72/0.634	29.94/0.833	29.45/0.827	28.53/0.768
(g) ASDS	(h) LMMSE	(i) NASR	(j) DPIR	(k) Zhang's + Denoising	(l) Ours
29.03/0.757	28.49/0.733	28.32/0.738	29.12/0.840	30.27/0.852	**30.39/0.859**

FIGURE 5. Comparison of SR results on Parrots image ($\sigma = 10$).

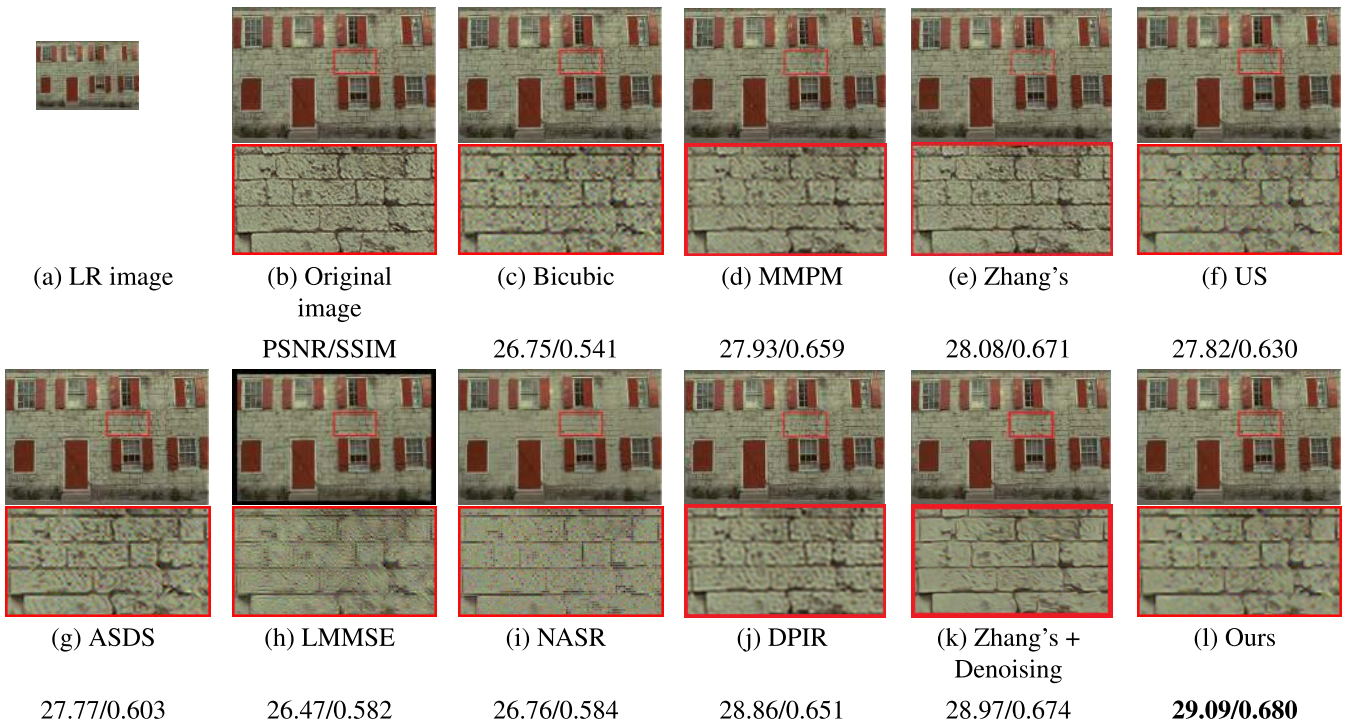| (a) LR image	(b) Original image	(c) Bicubic	(d) MMPM	(e) Zhang's	(f) US
	PSNR/SSIM	26.75/0.541	27.93/0.659	28.08/0.671	27.82/0.630
(g) ASDS	(h) LMMSE	(i) NASR	(j) DPIR	(k) Zhang's + Denoising	(l) Ours
27.77/0.603	26.47/0.582	26.76/0.584	28.86/0.651	28.97/0.674	**29.09/0.680**

FIGURE 6. Comparison of SR results on Wall image ($\sigma = 10$).

methods on Set5 and Set14 of all methods. Here, the PSNRs and SSIMs for color images are the average results of the red, green, and blue channels. Bold numbers represent the best performance.

In terms of the PSNR and SSIM values in Tables 1 and 2, our algorithm produces the best quantitative results compared with all baselines in most situations, especially the SSIM scores. The results demonstrates that the constructed
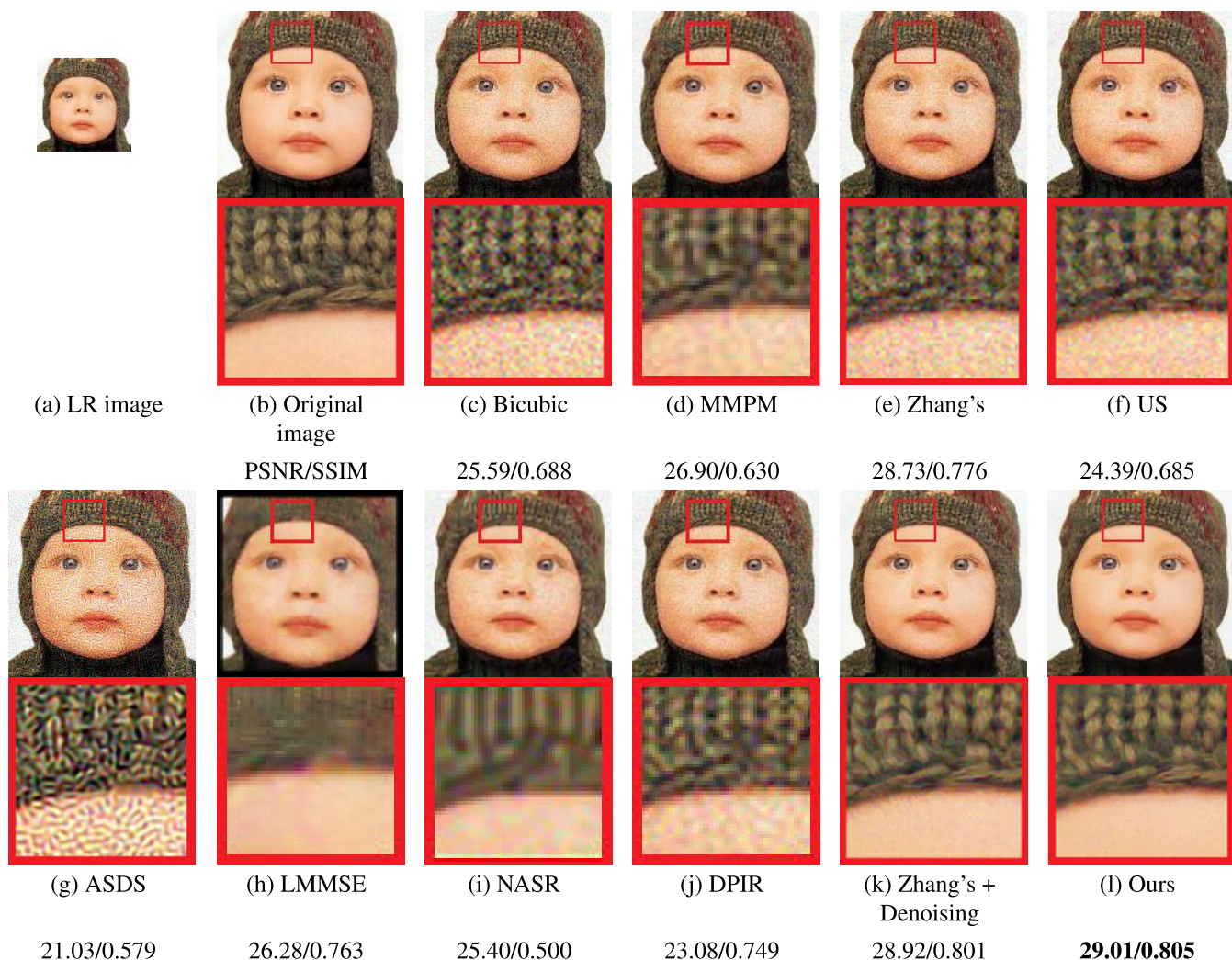
FIGURE 7. Comparison of SR results on Baby image ($\sigma = 20$).

(a) LR image	(b) Original image	(c) Bicubic	(d) MMPM	(e) Zhang's	(f) US
	PSNR/SSIM	25.59/0.688	26.90/0.630	28.73/0.776	24.39/0.685
(g) ASDS	(h) LMMSE	(i) NASR	(j) DPIR	(k) Zhang's + Denoising	(l) Ours
21.03/0.579	26.28/0.763	25.40/0.500	23.08/0.749	28.92/0.801	**29.01/0.805**

rational fractal interpolation model can well preserve the original image structure. Furthermore, the proposed method has obvious merits compared with other algorithms when the noise level is high. Thus, we can conclude that local fractal feature analysis is a quite efficient method for noisy image SR reconstruction.

To verify the effectiveness of our method in maintaining details, the edge preservation index (EPI) was used in the comparative experiments. This index is prone to noise level [29], whereas it can measure the ability of super-resolution operations on noise-less images to maintain image edges. The larger value of the index, the more details are retained. Table 3 shows the EPI results of the different methods on Set5 and Set14. Compared with the other methods, the proposed method achieves the highest EPI value on Set5. For the Set14 dataset, the proposed method also can also achieve excellent preservation of fine image details.

B. QUALITATIVE RESULTS

In Figs. 4-6, the subjective performance of the proposed technique and the other techniques is illustrated. To visually compare the effects of the different results, we show zoomed views of local regions of an image. Fig. 4 shows reconstructed results on noisy images (when $\sigma = 5$), and Figs. 5-6 show reconstructed results on noisy images (when $\sigma = 10$). As seen from visual comparisons, overall, the HR images reconstructed by our method have clearer textures, sharper edges and fewer artifacts than those of other state-of-the-art image SR methods.

Fig. 4 compares the reconstructed results of *Girl* image with $\sigma = 5$. Overall, compared with the other methods, the proposed method achieves better visual results in the image denoising and up-sampling. In the results reconstructed via bicubic interpolation, MMPM, Zhang's method and US, the noise is not satisfactorily removed. The images generated by ASDS and DPIR show fuzzy effects. LMMSE

and NASR fail to recover the texture details. Although Zhang's method with cascaded denoising can remove noise, the texture details cannot be well preserved by performing interpolation and denoising separately. In contrast, our method performs denoising and interpolation within the same framework and achieves satisfactory results for both texture preservation and denoising.

Fig. 5 compares the reconstructed results of *Parrots* image with $\sigma = 10$. Obviously, our method can produce a clearer and more detailed HR image. Bicubic interpolation, LMMSE and NASR generate many noise-caused artifacts. MMPM and Zhang's method can obtain better high-resolution images, but they cannot remove noise. Moreover, the texture details are not well maintained by Zhang's method with cascaded denoising. US, ASDS and DPIR can process the noise well; however, the smooth regions reconstructed via US are poorly contained, and ASDS and DPIR result in oversmoothed HR images. Fig. 6 shows the recovery effects achieved by the diverse algorithms on the *Wall* image with $\sigma = 10$. The results of bicubic interpolation, MMPM and Zhang's method are noisy. Overall, the other compared methods fail to distinguish information from noise to some extent and may produce undesired noisy results. In contrast, our approach is capable of obtaining vivid texture regions.

Fig. 7 compares the reconstructed results of *Baby* image with $\sigma = 20$. Visually, the proposed method achieves better results in terms of both image denoising and upsampling. The Bicubic interpolation, Zhang's method and US cannot remove noise. Moreover, the results of MMPM, LMMSE, NASR and Zhang's method with cascaded denoising are overly smooth. Compared with the results of ASDS and DPIR, the proposed method can obtain more highly detailed noiseless HR results.

In summary, the proposed algorithm can perform denoising and up-sampling simultaneously utilizing local fractal feature analysis. Specifically, for noisy image SR reconstruction, our constructed rational fractal interpolation model can efficiently preserve the original space characteristics of images. Moreover, using the LFD to describe image structure features is very suitable for achieving noisy image SR.

C. EFFICIENCY ANALYSIS

In this part, we compare the operating efficiency of the different methods. The experiments are implemented on Intel(R) Core(TM) i7-7600 3.40 GHz CPU with MATLAB R2017b. The average running time of different methods is shown in Table 4. ASDS, NASR and DPIR require large number of matrix calculations and iterative processes, which take a relatively long time. Compared with the Bicubic interpolation, MMPM, Zhang's method, US and LMMSE, although our method has a longer run time, it also achieves excellent denoising and SR performance. Overall, in light of the satisfactory denoising and SR results of the proposed method, its run time is considered acceptable.

VI. CONCLUSION

In this paper, we propose a novel method for noisy image SR within the framework of local fractal feature analysis, in which the LFD is used to describe the spatial features of images. Based on analysis of the degraded model, the developed method treats both upsampling and denoising as a problem and perform them under the same framework. A new rational fractal interpolation model with scaling factors is constructed that is highly suitable for noisy image interpolation. Then, by applying LFD image feature analysis for image denoising, a reconstructed HR image is free from noise-caused artifacts. Experimental results prove that our method is superior to other state-of-the-art methods both quantitatively and qualitatively. For the efficiency analysis of the proposed method, due to the longer running time used to analyze and calculate the fractal features of the input image, there is still room for improvement. Achieving satisfactory performance in a shorter run time will be a focus of our future research. For example, several acceleration techniques can be used to accelerate the proposed algorithm.

REFERENCES

[1] M. Bertero and P. Boccacci, *Introduction to Inverse Problems in Imaging*. Bristol, U.K.: IOP, 1998.

[2] H. Hou and H. Andrews, "Cubic splines for image interpolation and digital filtering," *IEEE Trans. Acoust., Speech, Signal Process.*, vol. ASSP-26, no. 6, pp. 508–517, Dec. 1978.

[3] K.-W. Hung and W.-C. Siu, "Robust soft-decision interpolation using weighted least squares," *IEEE Trans. Image Process.*, vol. 21, no. 3, pp. 1061–1069, Mar. 2012.

[4] L. Wang, H. Wu, and C. Pan, "Fast image upsampling via the displacement field," *IEEE Trans. Image Process.*, vol. 23, no. 12, pp. 5123–5135, Dec. 2014.

[5] H. A. Aly and E. Dubois, "Image up-sampling using total-variation regularization with a new observation model," *IEEE Trans. Image Process.*, vol. 14, no. 10, pp. 1647–1659, Oct. 2005.

[6] J. Sun, J. Sun, Z. Xu, and H.-Y. Shum, "Gradient profile prior and its applications in image super-resolution and enhancement," *IEEE Trans. Image Process.*, vol. 20, no. 6, pp. 1529–1542, Jun. 2011.

[7] L. Wang, S. Xiang, G. Meng, H. Wu, and C. Pan, "Edge-directed single-image super-resolution via adaptive gradient magnitude self-interpolation," *IEEE Trans. Circuits Syst. Video Technol.*, vol. 23, no. 8, pp. 1289–1299, Aug. 2013.

[8] R. Timofte, V. De Smet, and L. Van Gool, "A+: Adjusted anchored neighborhood regression for fast super-resolution," in *Proc. Asian Conf. Comput. Vis. (ACCV)*, Nov. 2015, pp. 111–126.

[9] J.-J. Huang and W.-C. Siu, "Learning hierarchical decision trees for single-image super-resolution," *IEEE Trans. Circuits Syst. Video Technol.*, vol. 27, no. 5, pp. 937–950, May 2017.

[10] Y. Huang, J. Li, X. Gao, L. He, and W. Lu, "Single image super-resolution via multiple mixture prior models," *IEEE Trans. Image Process.*, vol. 27, no. 12, pp. 5904–5917, Dec. 2018.

[11] W. Dong, L. Zhang, G. Shi, and X. Wu, "Image deblurring and super-resolution by adaptive sparse domain selection and adaptive regularization," *IEEE Trans. Image Process.*, vol. 20, no. 7, pp. 1838–1857, Jul. 2011.

[12] S. Mandal, A. Bhavsar, and A. K. Sao, "Noise adaptive super-resolution from single image via non-local mean and sparse representation," *Signal Process.*, vol. 132, pp. 134–149, Mar. 2017.

[13] F. Qiu, Y. Xu, C. Wang, and Y. Yang, "Noisy image super-resolution with sparse mixing estimators," in *Proc. 4th Int. Congr. Image Signal Process.*, Oct. 2011, pp. 1081–1085.

[14] L. He, J. Tan, X. Huo, and C. Xie, "A novel super-resolution image and video reconstruction approach based on Newton-Thiele's rational kernel in sparse principal component analysis," *Multimedia Tools Appl.*, vol. 76, no. 7, pp. 9463–9483, Apr. 2017.

[15] L. Zhang, X. Li, and D. Zhang, "Image denoising and zooming under the LMMSE framework," *IET Image Process.*, vol. 6, no. 3, pp. 273–283, Apr. 2012.

[16] Y. Xu, X. Yang, H. Ling, and H. Ji, "A new texture descriptor using multifractal analysis in multi-orientation wavelet pyramid," in *Proc. IEEE Comput. Soc. Conf. Comput. Vis. Pattern Recognit. (CVPR)*, Jun. 2010, pp. 161–168.

[17] Y. Xu, Y. Quan, H. Ling, and H. Ji, "Dynamic texture classification using dynamic fractal analysis," in *Proc. Int. Conf. Comput. Vis.*, Nov. 2011, pp. 1219–1226.

[18] Y. Wee and H. Shin, "A novel fast fractal super resolution technique," *IEEE Trans. Consum. Electron.*, vol. 56, no. 3, pp. 1537–1541, Aug. 2010.

[19] H. Xu, G. Zhai, and X. Yang, "Single image super-resolution with detail enhancement based on local fractal analysis of gradient," *IEEE Trans. Circuits Syst. Video Technol.*, vol. 23, no. 10, pp. 1740–1754, Oct. 2013.

[20] B. B. Mandelbrot, "Self-affine fractals and fractal dimension," *Phys. Scripta*, vol. 32, no. 4, pp. 257–260, 1985.

[21] S. Novianto, Y. Suzuki, and J. Maeda, "Near optimum estimation of local fractal dimension for image segmentation," *Pattern Recognit. Lett.*, vol. 24, nos. 1–3, pp. 365–374, Jan. 2003.

[22] K. Zhang, Y. Li, W. Zuo, L. Zhang, L. Van Gool, and R. Timofte, "Plug-and-play image restoration with deep denoiser prior," Aug. 2020, *arXiv:2008.13751*. [Online]. Available: http://arxiv.org/abs/2008.13751

[23] Y. Zhang, Q. Fan, F. Bao, Y. Liu, and C. Zhang, "Single-image super-resolution based on rational fractal interpolation," *IEEE Trans. Image Process.*, vol. 27, no. 8, pp. 3782–3797, Aug. 2018.

[24] B. B. Mandelbrot, *The Fractal Geometry of Nature*. New York, NY, USA: W. H. Freeman, 1982.

[25] W. K. Pratt, *Digital Image Processing*. Hoboken, NJ, USA: Wiley, 2001.

[26] A. Buades, B. Coll, and J.-M. Morel, "A non-local algorithm for image denoising," in *Proc. IEEE Comput. Soc. Conf. Comput. Vis. Pattern Recognit.*, Jun. 2005, pp. 60–65.

[27] M. Bevilacqua, A. Roumy, C. Guillemot, and M. L. A. Morel, "Low-complexity single-image super-resolution based on nonnegative neighbor embedding," in *Proc. Brit. Mach. Vis. Conf. (BMVC)*, Sep. 2012, pp. 135.1–135.10.

[28] R. Zeyde, M. Elad, and M. Protter, "On single image scale-up using sparse-representations," in *Proc. 7th Int. Conf. Curves Surf.*, Jun. 2010, pp. 711–730.

[29] J. Joseph, S. Jayaraman, R. Periyasamy, and S. Renuka, "An edge preservation index for evaluating nonlinear spatial restoration in MR images," *Current Med. Imag. Rev.*, vol. 13, no. 1, pp. 58–65, Jan. 2017.

QINGLAN FAN received the B.E. degree from the School of Information and Electrical Engineering, Ludong University, Yantai, China, in 2015, and the M.S. degree in computer application technology from the Shandong University of Finance and Economics, Jinan, China, in 2018. She is currently pursuing the Ph.D. degree with the School of Engineering and Computer Science, Victoria University of Wellington. Her research interests include image/video process and fractals.

YUNFENG ZHANG received the B.E. degree in computational mathematics and application software from the Shandong University of Technology, Jinan, China, in 2000, and the M.S. degree in applied mathematics and the Ph.D. degree in computational geometry from Shandong University, Jinan, in 2003 and 2007, respectively. He is currently a Professor with the Shandong Provincial Key Laboratory of Digital Media Technology, Shandong University of Finance and Economics. His current research interests include computer-aided geometric design, digital image processing, computational geometry, and function approximation.

FANGXUN BAO received the M.Sc. degree from the Department of Mathematics, Qufu Normal University, Qufu, China, in 1994, and the Ph.D. degree from the Department of Mathematics, Northwest University, Xian, China, in 1997. He is currently a Full Professor with the Department of Mathematics, Shandong University, Jinan, China. His research interests include computer-aided geometric design and computation, computational geometry, and function approximation.

CAIMING ZHANG received the B.S. and M.E. degrees in computer science from Shandong University, in 1982 and 1984, respectively, and the D.Eng. degree in computer science from the Tokyo Institute of Technology, Japan, in 1994. From 1997 to 2000, he held visiting position at the University of Kentucky, USA. His research interests include CAGD, CG, information visualization, and medical image processing.

KAI SHAO received the B.E. degree from the School of Computer Science and Technology, Shandong University of Finance and Economics, Jinan, China, in 2018. He is currently pursuing the M.S. degree with the Shandong Provincial Key Laboratory of Digital Media Technology, Shandong University of Finance and Economics. His research interests include medical image processing and deep learning.

• • •